Journal of Power Sources 262 (2014) 93–103

Contents lists available at ScienceDirect

Journal of Power Sources

journal homepage: www.elsevier.com/locate/jpowsour

The five modes of heat generation in a Li-ion cell under discharge

Rengaswamy Srinivasan*, A. Carson Baisden, Bliss G. Carkhuff, Michael H. Butler

Applied Physics Laboratory, The Johns Hopkins University, Laurel, MD 20723-6099, United States

HIGHLIGHTS

- Li-ion cell under discharge generates thermal energy through five different modes.
- Three of the five modes are the electrolyte, anode, and cathode resistances.
- Two of the five modes are the entropy change in the cathode and the anode.
- The five are dependent on the rate of discharge and the environmental temperature.
- Measurement and quantification of heat generated by each mode is demonstrated.

ARTICLE INFO

Article history:
Received 5 December 2013
Received in revised form
14 March 2014
Accepted 17 March 2014
Available online 27 March 2014

Keywords:
Li-ion cell
In situ tracking of thermal runaway
Noninvasive sensors
Resistive heating
Entropy-generated heating

ABSTRACT

A lithium-ion cell under discharge generates thermal energy (Q) through five different internal parameters or modes: the electrolyte resistance (R_s), anode resistance (R_a), cathode resistance (R_c), and entropy changes in the cathode (ΔS_c), and the anode (ΔS_a). This work demonstrates a set of tools to measure/quantify the heat generated by each parameter separately during discharge. These five sources are not dependent upon each other; they are dependent on the state of charge and the environmental temperature (T_{env}). The Q generated by each mode varies with degree of discharge and T_{env}. R_s generates most of the Q in the −10 °C to 40 °C range; R_c becomes significant at T_{env} <20 °C. Constant current discharge does not cause a monotonic increase in anode and cathode temperatures (T_a and T_c), due to the direction of change in ΔS_c and ΔS_a. Negative change in ΔS_a for the carbon anode cools it, causing the T_a to level off and even decrease with increased discharge. ΔS_c for lithium manganese oxide cathode is positive at some SoC and negative at others, preventing a monotonic increase in T_c. Measuring the five Qs separately opens the opportunity to study thermal-runaway from the perspective of the anode, cathode and electrolyte.

1. Introduction

Lithium-ion cells are among the optimal electrical energy storage and power delivery devices. During each charge–discharge cycle, the cell converts electrical energy into chemical and thermal energies; the cell is only capable of storing the chemical energy. The discharge reverses the process, converting the chemical energy into electrical and thermal energies. The thermal energy generated by the cell during charging and discharging is permanently lost, never stored or recovered as electrical or chemical energies, and accounts for the energy loss experienced during every charge–discharge cycle. Thermal energy generated inside the cell increases the internal temperature of the cell and under extreme conditions can initiate other exothermic chemical reactions causing the cell to vent, and sometimes transitioning the cell to a thermal runaway condition. Venting and thermal runaway are major safety issues related to Li-ion cells, and their causes and ramifications can be found in recent reviews and news articles [1,23].

The most common and accepted modes of thermal energy (Q) generation during charging and discharging of Li-ion cells are entropy- and internal resistance-related, and researchers use indirect measurements and thermal models to estimate the magnitude of Q [4–6]. The more direct measurements of Q are made using calorimeters [7–9]. However, such measurements only yield the sum of all the heats, not the individual components of the heat generated inside the cell.

It has been commonly recognized that the heat is generated through five different modes by five independent components inside the cell [5–7]. They are: i) the electrolyte resistance (R_s);

* Corresponding author. Tel.: +1 443 778 6378; fax: +1 443 778 5937.
E-mail addresses: Rengaswamy.srinivasan@jhuapl.edu, srinir@comcast.net (R. Srinivasan).

http://dx.doi.org/10.1016/j.jpowsour.2014.03.062
0378-7753/

ii) the anode resistance (R_a); iii) the cathode resistance (R_c); iv) the entropy change in the cathode (ΔS_c); and v) the entropy change in the anode (ΔS_a). The rate of heat generated by each one of these five modes is dependent upon the temperature of the cell, and the amplitude and direction of the current. The ability to measure the individual contribution by each mode to Q, especially during the course of charging and discharging, yields invaluable information about the thermal behavior of each mode. It is, perhaps, the most successful way to track all the vital points inside the cell, and provide a trajectory for any impending errant behavior by the cell.

The major focus of the work described below is to quantify the contributions by the individual modes to the thermal energy outputted during discharge, and to reconcile those individual contributions with the overall thermal behavior of the cell during discharge. In addition, the work also demonstrates: i) the instantaneity of the impact of the changes in the discharge current on T_a and T_c; ii) ultraslow responses of the surface temperature (T_{surf}) to the changes in the current; and iii) inhomogeneity in the temperature within the cell, namely, differences between the T_a and T_c during discharge; and iv) presence of correlation between T_a and T_c with T_{env}, and absence of correlation between the T_{surf} and T_{env}.

1.1. Highlights of the techniques used in online monitoring of heat generation

Two different techniques are available to estimate the heat energy generated by each of the five modes. For estimating the entropy-related thermal energy, we used a recently-acquired technique that allows one to measure T_a and T_c in situ, while the cell is under charge and discharge [10]. By measuring, for example, T_c, one could compute $Q_{\Delta S_c}$, the heat associated with the entropy change in the cathode (ΔS_c); similarly, $Q_{\Delta S_a}$ by measuring T_a. On the other hand, for estimating the Joule heating, one would need the R_a, R_c, and R_s values measured during discharge.

The R_a, R_c, and R_s values can be obtained using conventional electrochemical impedance spectroscopy (EIS). The technique to measure T_a and T_c is also based on impedance. A measure of the phase shift (ϕ) between an applied voltage (or current) and the resultant current (or voltage) at a single frequency is a function of

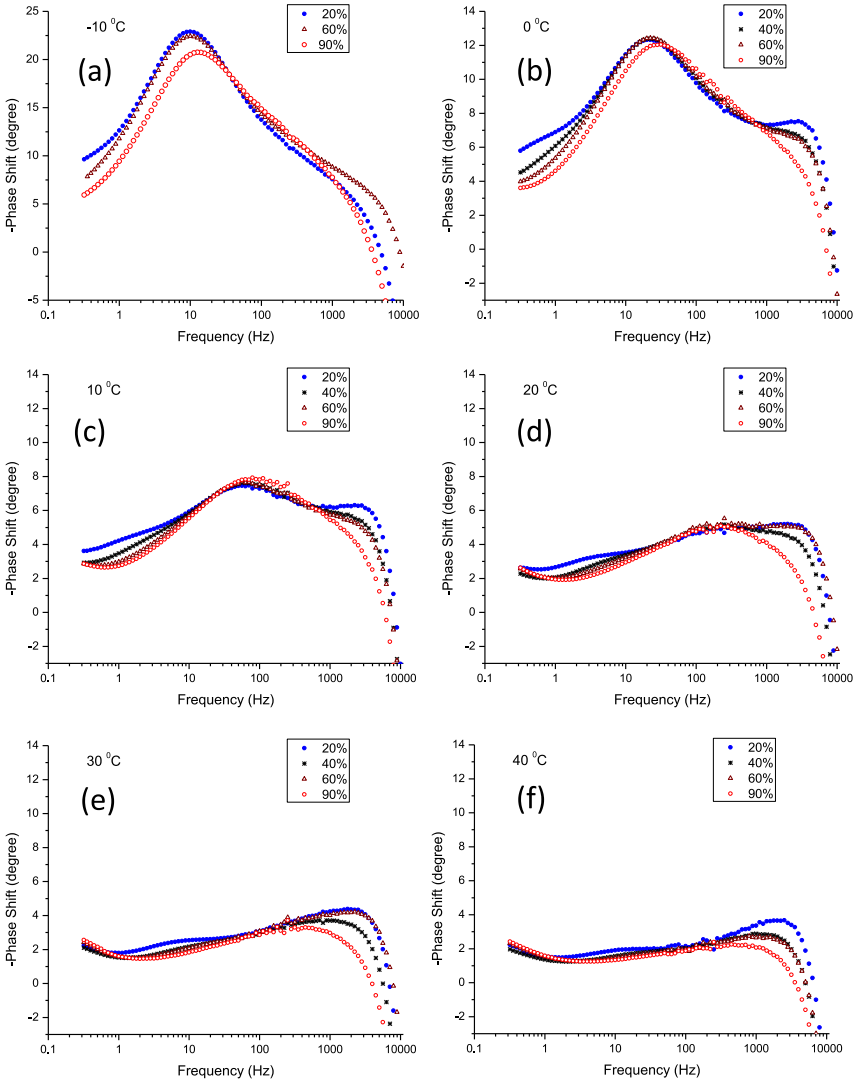

Fig. 1. Bode plots showing phase shift, ϕ, versus frequency for a 4.4-Ah Swing 4400 Li-ion cell at different SoC in six different T_{env} from −10 °C to 40 °C as indicated in (a)–(f). The value of ϕ at 20 Hz represents the T_c, and at 100 Hz represents T_a. Note that at all frequencies between 20 Hz and 200 Hz, ϕ is insensitive to SoC and sensitive to T_{env}. The associations of the values of ϕ to T_c at 20 Hz and to T_a at 100 Hz are explained in Fig. 4.

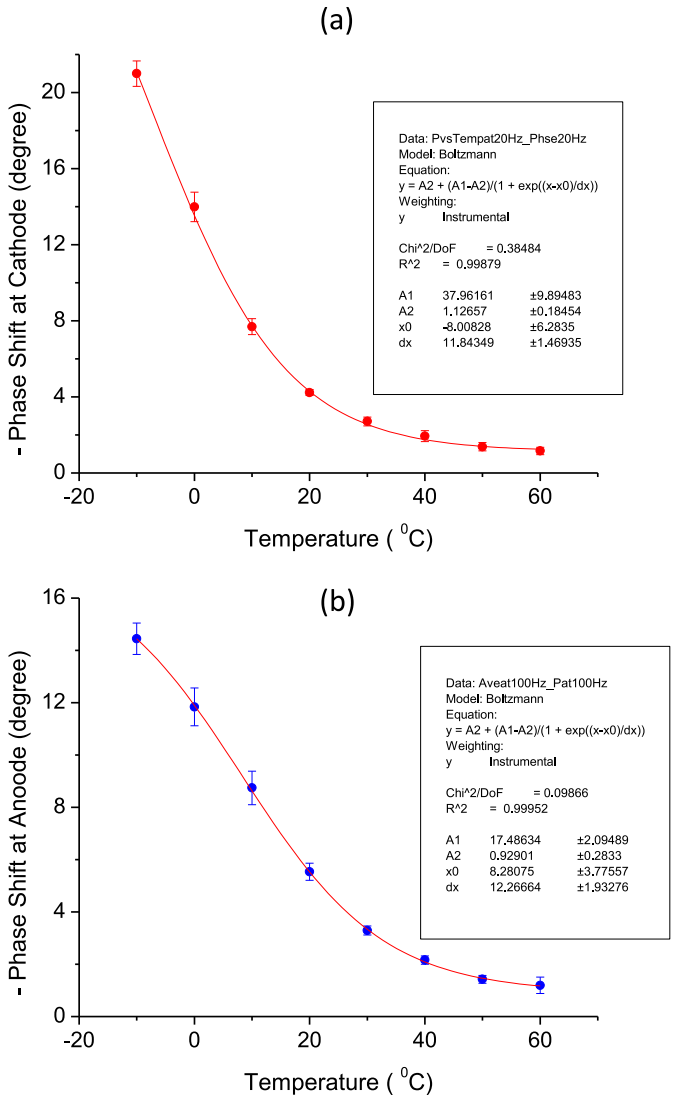

Fig. 2. The ϕ versus temperature calibration curves for: (a) T_c, using the ϕ values measured at 20 Hz; and (b) T_a, using the ϕ values measured at 100 Hz. Each point in the graph is the average of eleven measurements at eleven different SoCs between 5 and 95%. The lines represent polynomial fits to the measured data.

the temperature; for most Li-ion cells tested (capacity: 1-Ah–55-Ah), the ideal frequency for measuring T_c is in the 10- to 30-Hz range, and for T_a in the 40- to 100-Hz range [11].

Note that the capacitive and resistive properties of the anode and the cathode are quite different from each other, such that ϕ is responsive to T_a in the high-frequency range and to T_c in the low-frequency range. Most importantly, the frequency range where ϕ is only sensitive to T_a is well separated from the range where ϕ is only sensitive to T_c; and over these two ranges, the phase values are insensitive to the cell's state-of-charge (SoC). More specifically, at any one frequency in the 40- to 100-Hz range, ϕ is responsive to T_a; and in the 10- to 30-Hz range, it is responsive to T_c [11–13].

The impedance-based approach to T_a and T_c measurements provides several unique advantages over the fiber optic-based internal temperature sensors that are currently under development [14]. The fiber optic sensor is invasive. If it is too thick (several microns), it will seriously interfere with the current density distribution between the anode and the cathode, and if it is too thin, it will be too quickly etched by the multiple chemicals (oxidizers and reducers) that are present inside the Li-ion cell. By contrast, the impedance-based phase measurement is truly noninvasive: it is an electrical technique, and it uses electrical wires to connect to the positive and negative terminals of the cell to monitor T_a and T_c. Furthermore, the technique facilitates measuring T_a and T_c separately therefore the thermal properties of the anode and cathode can be assessed separately or independent of each other.

2. Methods

Measurements of heat generation during constant-current discharge at C-rate (4.4-A rate) were conducted on freshly procured 4.4 Ah Boston Power Swing 4400 cells. Electrical contacts to the cell were made through nickel tabs welded to the cell's positive and negative terminals. The anode in the cell is composed of graphite; the cathode is lithium manganese oxide. The freshly obtained cells were first subject to two or three charge–discharge cycles. Next, the cells' capacities at different temperatures were determined by cycling them at the manufacturer-specified charge–discharge rates using a programmable battery tester (Arbin Instruments Model BT2000). During the tests, the cells were housed inside an environmental chamber (Tenney Model: TJR); air circulation inside the chamber facilitated active heat transfer between the cell surface and the surrounding. A surface-mounted K-type thermocouple monitored the cell's surface temperature, T_{surf}. Prior to each discharge, the cells were first discharged to 2.7 V cut-off and charged to full capacity at room temperature (23.5 °C), and next kept up to 5 h in an environmental thermal chamber at the designated T_{env} in order to ensure equilibration between the cell's internal temperature T_{env}. Finally, after the discharge to the 2.7 V cut-off value at each T_{env}, the cell temperature was equilibrated with the room temperature over 12 h, and re-discharged at C/4 rate from its open circuit voltage to a 2.7 V cut-off; this procedure yielded the residual electrical energy (E_{d2}) that was left un-discharged during the first discharge at the T_{env}. The heat energy generated during the second discharge (for estimating E_{d2}) was assumed negligible.

During the course of charge and discharge, the cell impedance (EIS) and phase shifts were measured using a Solartron Model Electrochemical Interface (potentiostat/galvanostat) Model SI 1287, and Frequency Response Analyzer Model SI 1250. The frequency (f) range for the EIS measurement was set to span from 0.8 Hz to 10 kHz, for a total of 45 individual frequencies. The amplitude of the perturbation current, i_{ac} was set at 50 mA rms; this perturbation current caused no more than a 1-mV polarization to the cell voltage, V_{ac}. T_a and T_c, as well as R_s, R_a and R_c values were derived from the EIS data.

3. Results and discussions

The discussions below are centered on the measurement of thermal energy generated during discharge by five independent modes: R_s, R_a, R_c, ΔS_c and ΔS_a; and their dependence on T_{env}. The ability to measure T_a and T_c during discharge allowed us to estimate $Q_{\Delta S_c}$ and $Q_{\Delta S_a}$. Similarly, the ability to monitor R_s, R_a and R_c during the course of discharge enabled us to estimate the individual contributions by the three modes to Joule heating. The impedance technique, in conjunction with the use of electrical equivalent circuits to measure R_s, R_a and R_c, is a classical method to probe Li-ion cells, and is amply described in textbooks [15]. The technique to measure T_a and T_c is relatively new therefore important details of the technique along with the results are described in the next subsection.

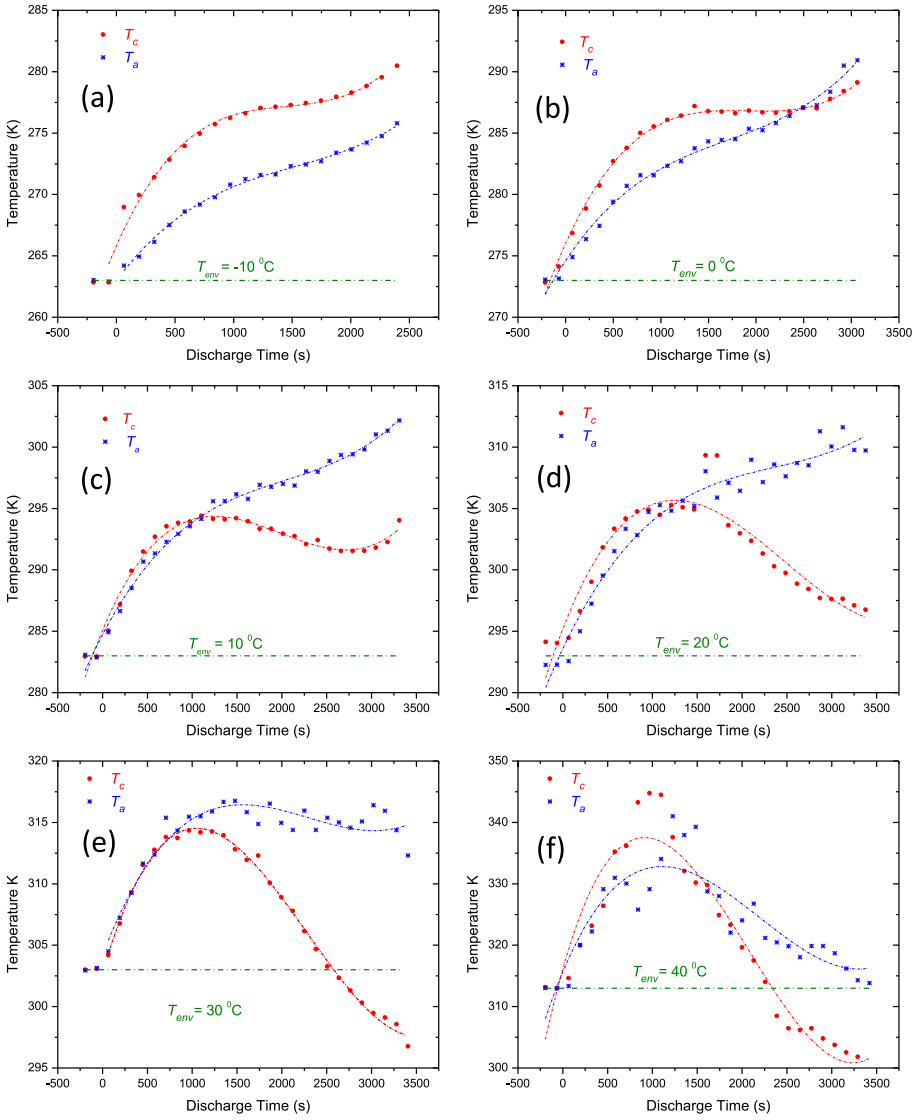

Fig. 3. Internal temperature data collected during the discharge of the 4.4-Ah cell at 4.4-A rate in six different T_{env} from −10 °C to 40 °C as indicated in (a)–(f). The dots are the experimental T_c and T_a values measured in intervals of 129.4 s. The dotted lines are polynomial fits to the experimental data.

3.1. Phase shift versus T_a and T_c

The technique used in measuring T_a and T_c is based on electrical phase (ϕ) measurement. The unique relationships between ϕ and T_a; and ϕ and T_c are demonstrated in Fig. 1 through the phase shift versus frequency (ϕ vs. f) data collected at 20%, 40%, 60% and 90% SoC at different T_{env} in the −10 °C to 40 °C range. Note that while collecting the data shown in the figure, the cell was not under charge or discharge in order to avoid current-induced heat generation inside the cell. We also assumed that the sub-microwatt heat generated by the 50-mA ac current used in perturbing the cell during the ϕ measurement is too small to affect T_a and T_c. Prior to each ϕ measurement, the cell was allowed to equilibrate with T_{env} for two to five hours.

At each temperature, in the 10-Hz–700-Hz range, the values of ϕ are found to be virtually independent of SoC and strongly dependent on T_{env}; at $f <$ 10-Hz, the ϕ values are dependent on SoC therefore the phase data at $f <$ 10-Hz should not be used to measure T_a or T_c. Note that the data shown in the figure were collected by first setting the cell at a given SoC, then allowing its internal temperature to equilibrate with T_{env} in a thermal chamber for several hours, and then measuring the ϕ values; most importantly, after setting the SoC at a fixed value, for the entire duration of temperature equilibration and ϕ measurements, the cell was guarded against charging or discharging. To minimize self-discharge loss of stored energy, all tests were completed within 2 days of charging, Next, an arithmetic mean of ϕ at multiple SoC in the 5%–95% range provided a single data-point in a calibration curve of "ϕ versus T_a" (for example, at $f = 100$ Hz) and "ϕ versus T_c" (for example, at $f = 20$ Hz). Repeating such measurements over a wide range of temperatures range constitutes a complete ϕ versus T_a and ϕ versus T_c calibration curves. More details of this procedure to obtain ϕ versus T_a calibration curve are described in Ref. [11]. The ϕ vs. T_a and ϕ vs. T_c calibration curves made on a new Swing 4400 cell are shown in Fig. 2. Note that one set each of calibration for T_a and T_c is sufficient for given cell model to measure its internal temperatures, T_a and T_c under static (no charge or discharge) and dynamic (during charging and discharging) conditions.

Fig. 3 shows the T_a and T_c values estimated using ϕ measurements, in intervals of 129.4 s while discharging the cell at 4.4-A

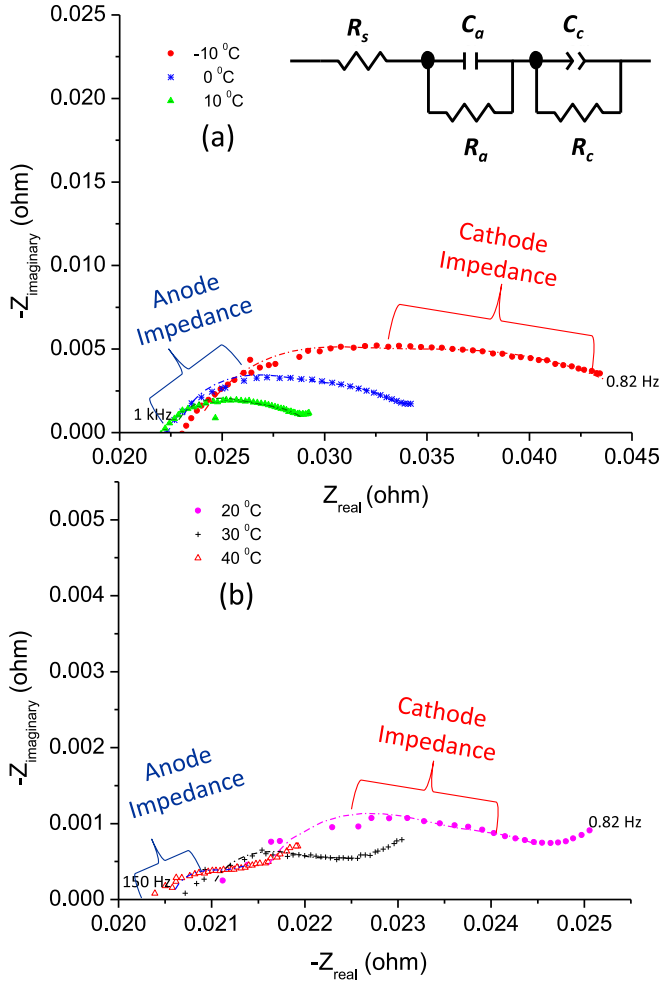

Fig. 4. Impedance of the 4.4-Ah Li-ion cell at various T_{env} as indicated. For clarity, only one set of impedance at one SoC (60%) at each of the six T_{env} are shown in two figures (a) and (b). Each point in the graph represents impedance data at one of about 45 separate frequencies, f between 0.82 and 1000 Hz (or 150 Hz); the end frequencies are shown in the figure. The dotted lines are mathematical fits to the experimental data, obtained using the electrical equivalent circuit shown in the inset in (a). The approximate data points in each graph, representing the cathode and the anode impedances, are shown using double brackets.

rate; note that prior to each discharge, in order to ensure accuracy and reproducibility of the impedance and ϕ measurements, the test cell was first fully charged, and then its internal temperature was equilibrated with T_{env} for several hours in an environmental thermal chamber.

3.2. R_a, R_c and R_s estimations from impedance measurement

During discharging, a cell's SoC and the temperatures of its internal components (anode, cathode and the electrolyte) do change. Our goal is to estimate the individual thermal energy generated through Joule heating by R_a, R_c and R_s while the cell is under discharge. A feasible path to the estimation is through a measure of the cell's internal impedance at multiple frequencies (in the 1-Hz–10-kHz range), under the dynamic condition of discharge. Note that at the discharge rate of 4.4-A, a fully-charged 4.4-Ah cell will discharge in roughly 1 h. During the course of discharge at each T_{env}, we made about 30 sets of impedance measurements at the rate of about 129.4 s per set. One such set at each T_{env}, for a total six sets, are shown in Fig. 4. Also shown in the figure are the mathematical fits to the data at each T_{env}, and the electrical equivalent circuit used in arriving at those fits. The fit yields R_a, R_c and R_s, and by repeating the fit over all the sets at T_{env}, (roughly a total of 180 sets of impedance data), we obtained about 500 values of R_a, R_c and R_s at the six different T_{env}; the results are shown in Fig. 5.

Note that R_a has a weak dependence on SoC [16]; R_c has a stronger dependence on SoC, while R_s is also weakly dependent on SoC, as may be seen from Figs. 1 and 2 in Ref. [11]. Due to the varying dependence of R_a, R_c and R_s on SoC, in Fig. 5 and in several subsequent figures that involve the three resistances, we chose to represent their dependence on temperature as a function of discharge time.

3.3. ΔS_a and ΔS_c estimations from literature data

Entropy-related thermal energy ($Q_{\Delta S}$) is obtainable through the relationship $Q_{\Delta S} = -T\Delta S$. Thus, to estimate $Q_{\Delta S}$ due to the anode and cathode, we need two parameters for each electrode: T and ΔS. Neither T nor ΔS remain constant during the course of discharge therefore should be obtained throughout the course of discharge. The procedure to obtain T_a and T_c values online, i.e. while discharging the cell, was described in Section 3.1. The technique available to measure ΔS is much slower than impedance measurement therefore monitoring it during discharge is virtually infeasible; details about estimating ΔS at different SoC (under static conditions only: no charging or discharging) are described in the published literature [5,17–19]. Fortunately, ΔS is not dependent on discharge rate or T_{env}; it is only dependent on SoC. The published literature is abundant with ΔS_a for various types of carbon, the anode material, and ΔS_c for different types of cathode material.

Part of the cathode material in the Swing 4400 cell is lithium manganese oxide (LMO); a closely matching material is lithium in spinel manganese oxide for which the ΔS_c vs. SoC due to the intercalation of lithium was estimated by Yazami et al. [18] The anode material in the Swing 4400 cell is graphite; we assumed the ΔS_a vs. SoC data estimated by Reynier et al. as a close approximation [17]. The ΔS_c vs. SoC and ΔS_a vs. SoC sets estimated by the Yazami–Reynier team are discrete values measured at large intervals of SoC. We fit their data to a polynomial approximation (Fig. 6) and interpolated the data needed in the required intervals of SoC for the 4.4-Ah cell discharging at 4.4-A rate.

3.4. Contributions by R_s, R_a, R_c, ΔS_c and ΔS_a to heat generation

The major goal of this work has been to demonstrate an approach to measure the individual contributions by the five modes, R_s, R_a, R_c, ΔS_c and ΔS_a, to the generation of thermal energy during the discharge of a Li-ion cell. Three of the five modes (resistances due to the electrolyte, R_s, anode, R_a, and cathode, R_c) were obtained using impedance technique; see Section 3.2 for details. Thermal energy generations due to the Joule heating were computed as i^2R_s, i^2R_a and i^2R_c, respectively for the electrolyte, anode and cathode; i represents the dc discharge current, which was fixed at 4.4 A. Thermal energy generations by the two other modes, the anode and cathode entropies, were obtained from the published literature data; see Section 3.3 for details. Computing the entropy-related thermal energy also required the anode and cathode temperatures that were measured using the phase-shift dependency on temperature; see Section 3.1 for details. The respective heat generations were computed as $(-T_a\Delta S_a)$ and $(-T_c\Delta S_c)$.

Fig. 7a through e provides a summary of the rate of heat generated (in units of Watt) during the constant-current discharge (4.4-A constant current) by each of the five modes. Each figure shows six different graphs corresponding to the heat data for one of the five modes, at six different T_{env}: −10 °C, 0 °C, 10 °C, 20 °C, 30 °C and 40 °C.

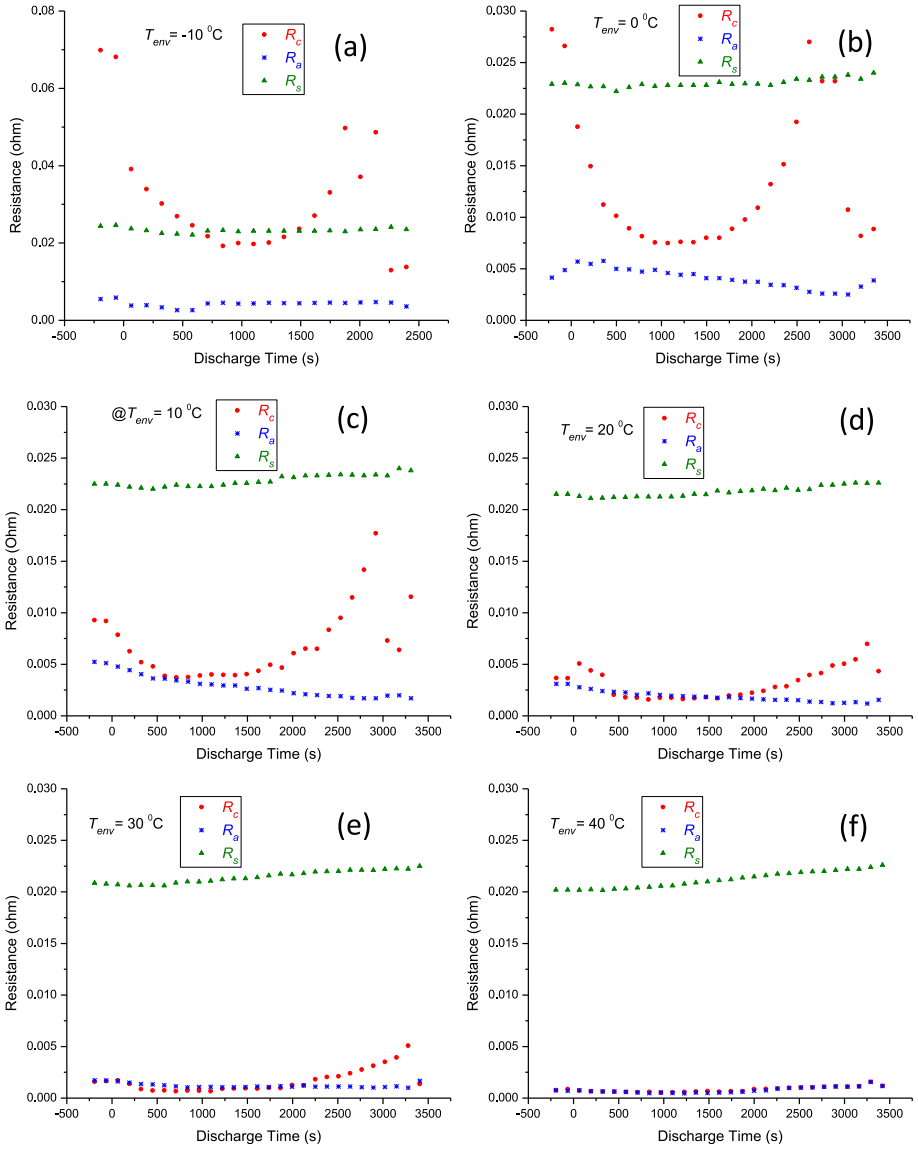

Fig. 5. Internal resistance data collected during the discharge of the 4.4-Ah cell at 4.4-A rate in six different T_{env} from −10 °C to 40 °C as indicated in (a)–(f). The dots are the experimental R_c, R_a and R_s values measured in intervals of 129.4 s.

The total rates of heat generated (in units of Watt) by all the five modes at each of the six T_{env} are shown in Fig. 7f. For each T_{env}, the area under the curve provides Q_{sum}, the integral of the heat generated (in units of Watt hour) by all the five modes during the entire course of discharge at that T_{env}. In other words, at each T_{env}, $Q_{sum} = \int_0^\tau i^2 R_s dt + \int_0^\tau i^2 R_a dt + \int_0^\tau i^2 R_c dt + \int_0^\tau (-T\Delta S_a) dt + \int_0^\tau (-T\Delta S_c) dt$; where t is the discharge time; and τ is the total time to discharge from the fully charged state to 2.7 V cut-off, during constant-current discharge. Fig. 8 shows the Q_{sum} vs. T_{env}, as well as the integral of the thermal energy due to each of the five modes of heating.

The trend in Q_{sum} vs. T_{env} implies that the thermal energy, Q output during discharge decreases with increase in the environmental temperature; and for the cell model tested (Boston Power Swing 4400), the Q at 20 °C is identical to the heat generated by the electrolyte resistance, R_s at 20 °C. At lower T_{env}, the heat generation is higher, while the least amount is generated at higher T_{env}.

Note also that in Fig. 7a–f, the time to discharge to cut-off (2.7 V) is shorter at lower temperatures. This is due to the cell reaching the cut-off voltage sooner at lower temperatures. This also implies that even though the cut-off voltage is fixed at 2.7 V during discharge at all T_{env}, a fraction of the stored chemical energy remains un-discharged in the cell, and the magnitude of the un-discharged energy is higher at lower T_{env}; (see also Section 5).

The implications of the observations posted in Figs. 7a–f and Fig. 8 are elaborated next.

4. Manifestations of R_s, R_a, R_c, ΔS_c and ΔS_a on the thermal behavior during discharge

It is obvious from the data in Figs. 5 and 6 that any T_{env}, the five internal properties, R_s, R_a, R_c, ΔS_c and ΔS_a, vary widely over SoC and the time-of-discharge. Therefore, during discharge:

- The rate of heat generation by every one of the five modes will vary with time.

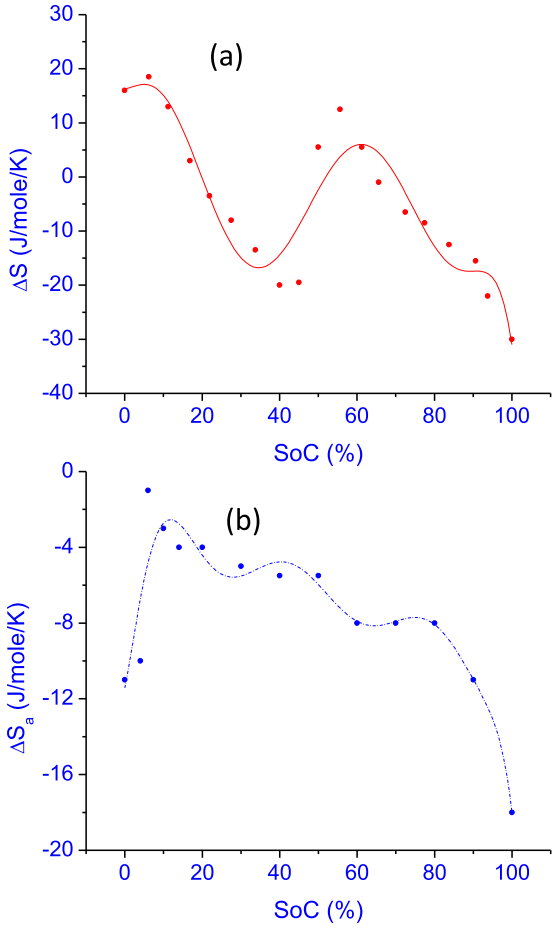

Fig. 6. Entropy changes across the SoC for: (a) LMO cathode; and (b) graphite anode. The dots are experimental data obtained from the published literature [17,18]; and the dotted lines are polynomial fits.

- The variations do not follow any particular behavior or law (linear, exponential, parabolic, etc.).
- It is therefore infeasible to generate predictive models for the thermal behavior of a Li-ion cell under discharge.
- Continuous monitoring of R_s, R_a, R_c, T_c and T_a during the discharge is the only way to measure the heat generated by each mode and each component (anode, cathode and electrolyte) of the cell.

Some of the nuanced aspects of the non-linear dependency of the five modes of heat generation on SoC and temperature are described next with reference to Joule and entropy heating.

4.1. Joule Heating

Comparing R_s, R_a and R_c with each other, the electrolyte resistance:

- R_s is the only parameter that is almost invariant with T_{env}, staying within the range of 0.02 Ω–0.024 Ω across all SoC and the T_{env} range (−10 °C and 40 °C).
- R_c varies most, from 0.0006 Ω (at T_{env} = 40 °C) to 0.05 Ω (at T_{env} = −10 °C). At $T_{env} \leq 0$ °C, the cathode resistance R_c is comparable to and even higher than the electrolyte resistance, R_s.
- R_a has the least magnitude of the three, never increasing above 0.006 Ω.
- Within the 45% and 90% SoC range, R_s, R_a and R_c all show a minima implying that the three resistances will generate the least amount of heat within this range of the SoC.
- R_s dominates over R_a and R_c, therefore the electrolyte is responsible for most of the resistive heat generation.

4.2. Entropy-assisted heating and cooling

Comparing $-T_c\Delta S_c$ and $-T_a\Delta S_a$ with each other, (Fig. 7d and e):

- The anode always cools due to the entropy change in the anode; such a behavior of the anode is common to all Li-ion cells that uses carbon anode.
- On the other hand, the LMO-based cathode behavior is more complex, whose ΔS_c changes in the positive and negative directions over the SoC range of full charge to full discharge [18]. Thus, ΔS_c tends to heat the cathode in certain ranges and cool it in others.

4.3. Influence of Joule and entropy on T_a and T_c

The sum $(i^2R_c + (-T_c\Delta S_c))$ influences, at least partially, the T_c, the temperature of the cathode; similarly, $(i^2R_a + (-T_a\Delta S_a))$ influences T_a. However, the resistive heating by the electrolyte has stronger role in determining the temperature of the anode and cathode for most part, though not entirely. The dominance of R_s over R_c and R_a, and the proximity of the electrolyte to the anode and the cathode, do play a role in increasing T_a and T_c during the initial stages of discharge. However, the entropy-based thermal properties, $-T_c\Delta S_c$ and $-T_a\Delta S_a$ do play a major role in modulating T_a and T_c. Note from Fig. 7, the heating rate due to i^2R_s is almost constant, increasing by less than 10% over the entire course of discharge. On the other hand, the rate of heating due to all the other modes varies more widely, and while cooling in some places. The modulations in T_c can be explained by the fluctuations in $(i^2R_c + (-T_c\Delta S_c))$ vs. SoC; and those in T_a by the changes in $(i^2R_a + (-T_a\Delta S_a))$ vs. SoC.

Fig. 9a–f shows the sums of $(i^2R_c + (-T_c\Delta S_c))$ and $(i^2R_a + (-T_a\Delta S_a))$ through the course of discharge at all the T_{env}; also presented in each figure are the Joule heating by the electrolyte (i^2R_s) data for the purpose of comparison. Comparing them with the T_c data in Fig. 3 demonstrates the influence of $(i^2R_c + (-T_c\Delta S_c))$ on T_c. Almost at all T_{env}, past 2000 s of the C-rate discharge (SoC ≤45%), T_c begins to decrease from its maximum value. Starting at the 2000 s mark, $(i^2R_c + (-T_c\Delta S_c))$ has a negative slope or a decreasing rate of heating, followed by a negative sign or cooling past 2500 s (SoC ≤ 30%). By comparison, even though $(i^2R_a + (-T_a\Delta S_a))$ turns negative during discharge, due its relatively smaller amplitude, it does not influence T_a until $T_{env} > 30$ °C. In summary:

- The electrolyte resistance is least influenced by SoC and T_{env}, and it dominates the resistive heating and contributes most to T_c and T_a over much of the discharge.
- The entropy change in the cathode influences the T_c most below 45% SoC.
- Below 45% SoC, the entropy change in cathode is negative causing entropic cooling; however, only sufficiently to cause a small drop in the T_c; i^2R_c and i^2R_s continues to dominate over $(-T_c\Delta S_c)$, keeping the cathode hot.

5. The identity of stored energy at all T_{env} of discharge

Three sets of discharge energy data are needed to account for the manifestation of the chemical energy stored in the cell: the

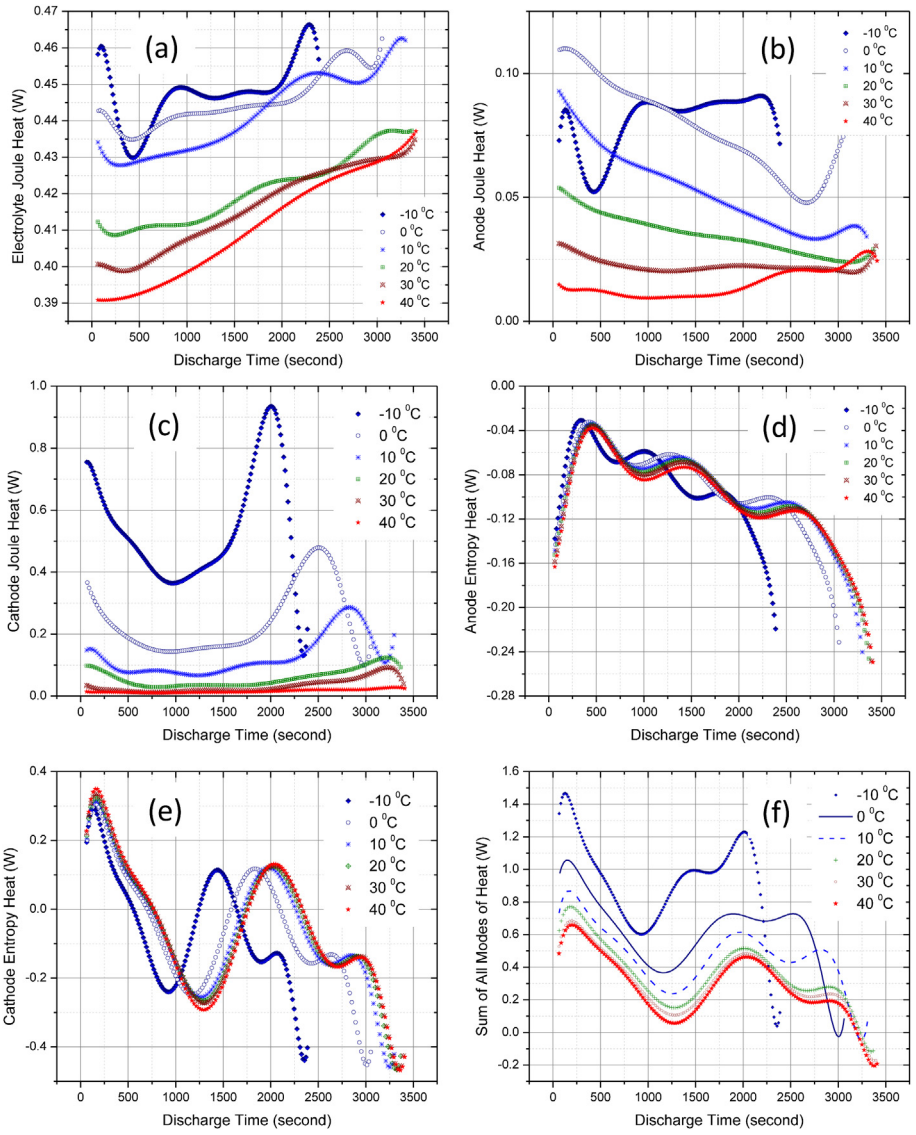

Fig. 7. Heat generated during discharge by the individual modes, R_s, R_a, R_c, ΔS_c and ΔS_a are shown in (a)–(e); and the sum of all the five modes in (f). Each figure has six graphs corresponding to measurements made at six different T_{env}.

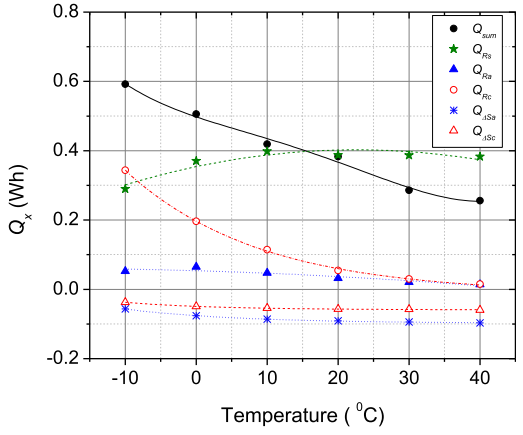

Fig. 8. The integral of the heat generated due to the individual modes ($\int_0^\tau i^2R_s dt$, $\int_0^\tau i^2R_a dt$, $\int_0^\tau i^2R_c dt$, $\int_0^\tau (-T\Delta S_a) dt$ and $\int_0^\tau (-T\Delta S_c) dt$, and their sum ($Q_{sum} = \int_0^\tau i^2R_s dt + \int_0^\tau i^2R_a dt + \int_0^\tau i^2R_c dt + \int_0^\tau (-T\Delta S_a) dt + \int_0^\tau (-T\Delta S_c) dt$) through the course of 4.4-A rate discharge, from full charge to the 2.7 V cut-off, at the six different T_{env}. The dots are the integrals obtained from experimental measurements, and the lines are polynomial fits.

electrical energy, thermal energy, and the energy that remained un-discharged due to the imposition of the 2.7 V discharge cut-off voltage during the discharge. The electrical energy E_{d1} is measured in terms of cell voltage, current and time during discharge. The Q_{sum} data in Fig. 8 is the thermal energy at each T_{env}. In order to measure the un-discharged energy after discharging at each T_{env}, following the discharge, we allowed the cell to equilibrate with the room temperature (23.5 °C) for 12 h, and then re-discharged the cell at a slow rate of 1.1-A to 2.7 V cut-off voltage. The electrical energy obtained during the second discharge, E_{d2} was assumed to be the entire un-discharged energy left behind during the first discharge; the thermal energy generated during the second discharge was assumed negligible. The results are shown in Fig. 10 that include the electrical energy (E_{d1}) and the thermal energy, Q_{sum} (obtained during the first discharge at each T_{env}), and the residual electrical energy, E_{d2} (obtained during the second discharge at 23.5 °C). Also shown in the figure is the $E_{deliverable}$: $E_{d1} + Q_{sum} + E_{d2}$. Note that $E_{deliverable}$ is nearly a constant at 14.4-Wh through all the T_{env}, which suggests at 14.4-Wh is the maximum amount of energy that the cell would ever deliver.

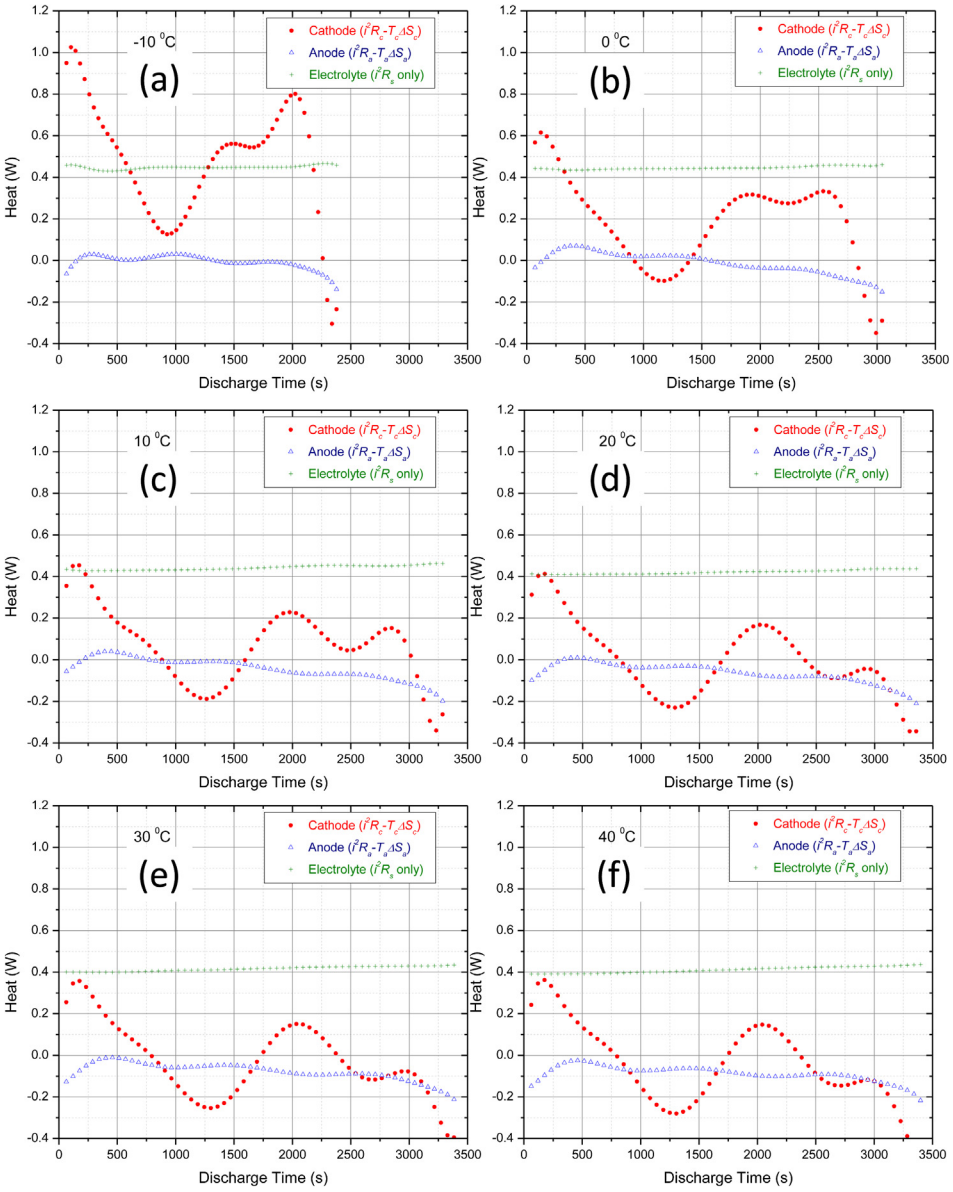

Fig. 9. Heat generated by the sum of resistive heating and the entropy changes in the anode ($i^2R_a + (-T_a\Delta S_a)$) and the cathode ($i^2R_c + (-T_a\Delta S_c)$) during discharge at different T_{env} as indicated in (a)–(f). Also shown are the heat generated by the resistive heating of the electrolyte (i^2R_s) at those T_{env}. Note that the heat data at $T_{env} = 30$ °C and 40 °C are similar, and not identical.

6. The disconnect between T_{surf} and the dynamics of heat generation

Most Battery Management Systems (BMS) use surface-mounted temperature sensors for the thermal management part. The data below show the potential disconnect between the surface temperature, T_{surf} and the thermal events in progress inside the cell under discharge.

First, the surface temperature lags behind the heat-generating events inside the cell by tens of seconds. Fig. 11 shows the T_a, T_c and T_{surf} for the 4.4-Ah cell discharging at 11-A rate in a 5 °C T_{env}. The T_a and T_c react to the current pulse almost instantaneously; the 15-s lag between the current pulse and the two temperatures is caused by the data collection rates for T_a and T_c. The T_{surf} increased sluggishly, not catching with T_a and T_c even after 60 s. Second, during discharge, there is virtually little correlation between T_{surf} and T_{env}, while T_c and T_a correlate well with T_{env}; see data in Fig. 12.

The data in the two figures suggest that the role of surface-mounted temperature sensors might need reevaluation to ensure reliable thermal management of rechargeable Li-ion batteries used in a wide range of equipment including electric vehicles, ships, commercial and military planes and satellites, especially when safety is utmost essential. In other words, surface-mounted temperature sensors should be replaced by internal temperature sensors for accuracy and reliability.

7. Conclusions

The paper describes a newly created capability to estimate in situ the heat generation from the perspectives of the individual components of a Li-ion cell, namely the anode, cathode and electrolyte. This capability is quite unlike that of the conventional calorimeters that are routinely used to report the heat generated by the entire cell, not their individual components. The sensors that

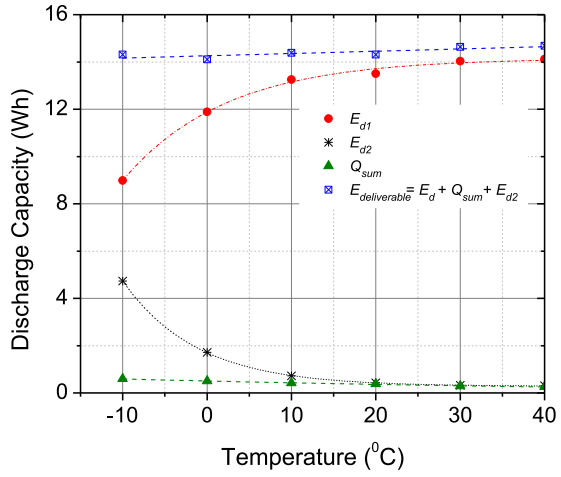

Fig. 10. During discharge at various T_{env}, the cell generates electrical energy (E_{d1}) and thermal energy (Q_{sum}). The part of the energy that remains un-discharged (E_{d2}) is higher at lower T_{env}. The sum of the three energies ($E_{deliverable}$: $E_{d1} + Q_{sum} + E_{d2}$) (the top curve) is nearly a constant at 14.4-Wh, most of which may be obtainable as electrical energy only at high T_{env}. At lower T_{env}, a part of the stored energy is left un-discharged in the cell. At all T_{env}, the thermal energy outputted during the C-rate discharge is only a fraction of the deliverable energy.

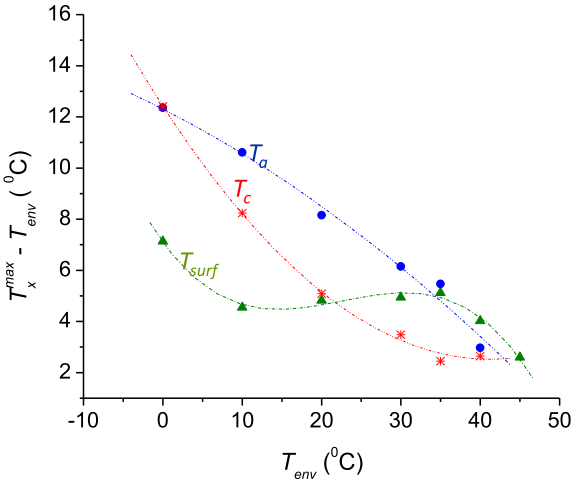

Fig. 12. The graphs demonstrate the absence of a non-monotonic association between T_{surf} with T_{env} that may pose challenges in the use of T_{surf} to predict the cell's internal temperatures while its surface is actively cooled. By contrast, the relationship between T_c and T_{env}, and T_a and T_{env} are monotonic. Moreover, the direct measurements of T_c and T_a remove the need to predict the internal temperatures. The T_x^{max} represent T_{surf}, T_c and T_a data measured at an arbitrary time during the 4.4-A discharge; the dots are experimental data and the lines are polynomial fits.

have empowered this new ability lend themselves for everyday use to track fire safety in lithium batteries, and they are quite unlike the conventional calorimeters that are relegated to laboratory use only.

The surface temperature (T_{surf}) of the cell lags so far behind its internal temperatures (T_a and T_c) that the relevance of monitoring T_{surf} to protect a cell against situations like thermal runaway is questionable.

Our work confirms that the rate of heat generation, Q by a Li-ion cell under discharge varies with discharge time, t, even if the discharge current, i and the temperature of the cell's environment, T_{env} are constant. In other words, Q vs. t is nonlinear, even if i vs. t and T_{env} vs. t are steady. The nonlinearity is caused by nonlinear dependence of the five modes responsible for the heat generation on temperature and SoC. The five modes are driven by five different material parameters of the cell: the resistances due to the electrolyte, anode and cathode, and the entropy changes in the anode and the cathode. Each parameter is dependent, to varying degrees, on temperature and SoC. Heat generated by some modes dominates at low T_{env}, while others, at high T_{env}. Most importantly, heat generation by each mode during discharge, behaves exactly as predicted by their respective property's dependence on T_{env} and SoC. This predictable behavior sets up an excellent opportunity to monitor heat generation during discharge and safeguard the Li-ion cell from thermal runaway.

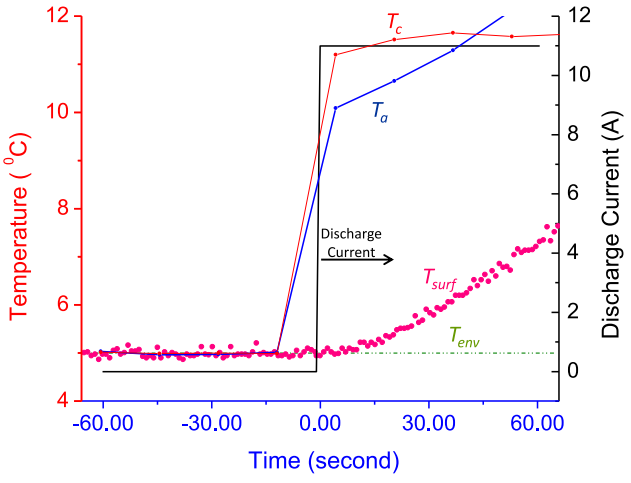

Fig. 11. The response of T_{surf} to a 2.5-C rate step current is rather sluggish, while the responses by T_a and T_c are much faster. Note that the rate of data collection for T_a and T_c was in 15-s interval; T_{surf} was collected at a much faster rate.

In a Li-ion cell under normal discharge, Joule heating due to R_s, R_c and R_a contribute to most of the thermal energy released. Of these three, R_s generates most of the heat, and R_a the least; and contribution by R_c varies with T_{env}: at low T_{env}, the heat generated by R_c is comparable and even higher than that by R_s, and at high T_{env}, it is small, comparable to that of R_a, and less than 3% of R_s.

Since variations in R_s, R_a, R_c, ΔS_c and ΔS_a with time of discharge are nonlinear, and do not follow any particular behavior or law such as linear, exponential, parabolic, etc., continuous monitoring of R_s, R_a, R_c, T_c and T_a during the discharge is the only way to measure the heat generated by anode, cathode and electrolyte. Fast tracking impedance technique is ideally suited for monitoring and safe guarding. This technique measures the electrolyte, anode and cathode resistances once every 2 min [20], and anode and cathode temperatures once every 1 s [13]. It is a suitable technique for monitoring heat generation, while the cell is under charge and discharge. The findings described in this work, and in Refs. [10,20,21] demonstrate a non-intrusive online technique to safeguard Li-ion batteries from venting, fire and thermal runaway. This novel approach of tracking the five modes of heat separately from each other opens a new path for in situ study of thermal-runaway in Li-ion cells.

Acknowledgments

The authors express their sincere gratitude to the Independent Research and Development programs by the National Security Space Mission Area and the Research and Exploratory Development Mission Area of the Applied Physics Laboratory (APL), the Johns Hopkins University for financial assistance. The authors would like to thank Dr. Rama Venkatasubramanian, APL and Dr. Margot Wasz, Aerospace Corporation, El Segundo, CA for valuable discussions.

One of the authors (RS) wishes to thank Janney Publication Program of APL for financial support to prepare the manuscript.

References

[1] P.G. Balakrishnan, R. Ramesh, T. Prem Kumar, J. Power Sources 155 (2006) 401–414.
[2] Q. Wang, P. Ping, X. Zhao, G. Chu, J. Sun, C. Chen, J. Power Sources 208 (2012) 210–224.
[3] R. Srinivasan, SPIE Newsl., 10 May 2013. http://spie.org/x93839.xml.
[4] V. Viswanathan, et al., J. Power Sources 195 (2010) 3720–3729.
[5] R.E. Williford, V.V. Viswanathan, Ji-Guang Zhang, J. Power Sources 189 (2009) 101–107.
[6] Gi-Heon Kim, et al., J. Power Sources 170 (2007) 476–489.
[7] A. Eddahech, Olivier Briat, Jean-Michel Vinassa, Energy 61 (2013) 432–439. A. Eddahech, O. Briat, J.-M. Vinassa, Lithium-ion Battery Heat Generation Investigation Based on Calorimetric Entropy Measurements, Proceedings of the ISIE, 2013 IEEE Industrial Symposium, 28–31 May 2013, Taiwan, http://dx.doi.org/10.1109/ISIE.2013.6563807.
[8] Yoshiyasu Saito, Masahiro Shikano, Hironori Kobayashi, J. Power Sources 244 (2013) 294–299.
[9] J. Singh, Thermal Runaway in Li-ion – Getting the Missing Data, vol. 40, BEST Magazine, Spring 2013, pp. 45–54.
[10] Rengaswamy Srinivasan, J. Power Sources 198 (2012) 351–358.
[11] R. Srinivasan, B.G. Carkhuff, M.E. Butler, A.C. Baisden, Electrochim. Acta 56 (2011) 6198–6204.
[12] R. Srinivasan, B.G. Carkhuff, M.E. Butler, A.C. Baisden, An External Sensor for Instantaneous Measurement of the Internal Temperature in Lithium-ion Rechargeable Cells, Proceedings of the SPIE conference on Defense, Security and Sensing, 25–29 April 2011. Paper No. 8035-13.
[13] R. Srinivasan et al., Battery Phase Meter to Determine Internal Temperatures of Lithium-ion Rechargeable Cells Under Charge and Discharge, US Patent Application Publication, 2012/0155507 A1, 21 June 2012; R. Srinivasan, B.G. Carkhuff, Control Apparatus and Methods for Conducting Fast Battery charge, US Patent Application Publication, 2013/0264999 A1, 10 October 2013.
[14] Peter Kiesel, Ajay Raghavan, SENSOR: Embedded Fiber-optic Sensing Systems for Advanced Battery Management, Advanced Energy Technology Congress, San Diego, CA, USA, November 12–15, 2013.
[15] David Linden, Thomas B. Reddy, Handbook of Batteries, third ed., McGraw-Hill, NY, 2002, pp. 2–26.
[16] P. Suresh, A.K. Shukla, N. Munichandraiah, J. Appl. Electrochem. 32 (2002) 267.
[17] Y. Reynier, R. Yazami, B. Fultz, J. Power Sources 119–121 (2003) 850–855.
[18] R. Yazami, Y. Reynier, B. Fultz, ECS Trans. 1 (26) (2006) 87–96.
[19] Y. Reynier, R. Yazami, B. Fultz, I. Barsukov, J. Power Sources 165 (2007) 552–558.
[20] R. Srinivasan, et al., Battery Health Monitor, Patent No. US 7,554,294, June 30, 2009.
[21] R. Srinivasan, B.G. Carkhuff, J. Power Sources 241 (2013) 560–566.

Glossary

C: capacity of a cell in units of ampere-hour (Ah)
C-rate: amplitude of current rated at the full capacity of the cell
$E_{deliverable}$: maximum deliverable energy (thermal + electrical) from a fully charge cell
E_{d2}: un-discharged energy left in the cell when the cell reaches the 2.7 V cut-off limit
f: frequency in Hz
i: discharge current
R_a: resistive impedance of the anode; it is a temperature-dependent parameter
R_c: resistive impedance of the cathode; it is dependent on temperature and SoC
R_s: resistive impedance of the electrolyte; it is weakly dependent on temperature and SoC
i^2R_a: Joule heating in anode in units of Watt (W)
i^2R_c: Joule heating in cathode in units of Watt (W)
i^2R_s: Joule heating in electrolyte in units of Watt (W)
LMO: lithium manganese oxide
ϕ: phase shift between the applied ac current and resultant ac voltage
ΔS: change in entropy
ΔS_a: change in entropy of the anode
ΔS_c: change in entropy of the cathode
τ: total time to discharge from the fully charged state to 2.7 V cut-off, during constant-current discharge
Q: heat generated by the cell during charging or discharging
$Q_{\Delta S}$: heat generated by change in entropy
$Q_{\Delta S_a}$: heat generated by change in anode entropy
$Q_{\Delta S_c}$: heat generated by change in cathode entropy
Q_{sum}: summed value of the integral of heat generated by each mode

$$((Q_{\mathrm{sum}} = \int_0^{\tau} i^2 R_{\mathrm{s}}\mathrm{d}t + \int_0^{\tau} i^2 R_{\mathrm{a}}\mathrm{d}t + \int_0^{\tau} i^2 R_{\mathrm{c}}\mathrm{d}t + \int_0^{\tau} (-T\Delta S_{\mathrm{a}})\mathrm{d}t + \int_0^{\tau} (-T\Delta S_{\mathrm{c}})\mathrm{d}t))$$

SoC: state of charge
t: time of discharge
T: temperature in K or °C
T_a: temperature of the anode
T_c: temperature of the cathode
T_{env}: temperature surrounding the outer surface of the cell, typically the temperature of the environmental chamber
T_{surf}: temperature at the outer surface of the cell measured by a K-type thermocouple mounted on the middle of the outer metal casing of the cell